nature geoscience

ARTICLES

https://doi.org/10.1038/s41561-018-0133-5

Tall Amazonian forests are less sensitive to precipitation variability

Francesco Giardina[1,2], Alexandra G. Konings[3], Daniel Kennedy[4], Seyed Hamed Alemohammad[4], Rafael S. Oliveira[5,6], Maria Uriarte[7] and Pierre Gentine[4,8]*

Climate change is altering the dynamics, structure and function of the Amazon, a biome deeply connected to the Earth's carbon cycle. Climate factors that control the spatial and temporal variations in forest photosynthesis have been well studied, but the influence of forest height and age on this controlling effect has rarely been considered. Here, we present remote sensing observations of solar-induced fluorescence (a proxy for photosynthesis), precipitation, vapour-pressure deficit and canopy height, together with estimates of forest age and aboveground biomass. We show that photosynthesis in tall Amazonian forests, that is, forests above 30 m, is three times less sensitive to precipitation variability than in shorter (less than 20 m) forests. Taller Amazonian forests are also found to be older, have more biomass and deeper rooting systems[1], which enable them to access deeper soil moisture and make them more resilient to drought. We suggest that forest height and age are an important control of photosynthesis in response to interannual precipitation fluctuations. Although older and taller trees show less sensitivity to precipitation variations, they are more susceptible to fluctuations in vapour-pressure deficit. Our findings illuminate the response of Amazonian forests to water stress, droughts and climate change.

Tropical rainforests play a crucial role in regulating the global climate system, representing the Earth's biggest terrestrial CO_2 sink. Because of its broad geographical extent and year-long productivity, the Amazon is key to global carbon and hydrological cycles[2]. Climate change could threaten the fate of rainforests[3], but there is large uncertainty about the future ability of rainforests to store carbon[4]. Severe droughts have occurred in recent years in the Amazon watershed[5–7], causing widespread tree mortality[8] and affecting the forests' ability to store carbon[9–12], yet the drivers of the sensitivity of tropical rainforests to drought are poorly understood. Future predictions of Amazon water stress vary widely according to the climate model used to predict precipitation[4]. In tropical areas, predicting future precipitation is more difficult as rainfall tends to be coupled to large-scale atmospheric wave dynamics and cannot be considered in isolation. Deforestation adds further uncertainty to this prediction.

Satellite observations have suggested that Amazon forests' photosynthesis was enhanced during drought[13]; however, it is likely that these findings have been affected by vegetation index measurement errors[14,15]. Recent in situ studies have shown that some areas of the Amazon exhibit higher photosynthesis towards the end of the dry season, indicating limited water stress[14–16]. Indeed, above a 2,000 mm yr^{-1} annual precipitation threshold, photosynthesis appears to be maintained during the dry season in tropical regions[17]. In addition to soil moisture and precipitation deficit, there is recent evidence of a substantial vapour-pressure deficit (VPD) effect in the mid-latitudes[18–20]. However, the sensitivity of tropical forest photosynthesis to VPD is unclear and even more poorly understood than the sensitivity to precipitation.

Large-scale studies of photosynthesis in Amazonia have mostly focused on seasonality and climatic drivers without considering the role of canopy heterogeneity[7,21,22], such as variability in forest height and age. Evidence from in situ studies suggests that tree size plays a role in drought response, with emergent trees exhibiting a weaker growth response to rainfall deficit than understory trees; however, larger trees also experience higher rates of mortality under drought[23]. These seemingly contradictory responses highlight our limited understanding of the drivers of photosynthesis in tropical forest ecosystems. Using remotely sensed solar-induced fluorescence (SIF) as a proxy for photosynthesis[24–26], we show that forest height variably influences the sensitivity of photosynthesis to precipitation. SIF has been shown to correspond to gross primary production (GPP) at large temporal and spatial scales[25,26]. We find that tall and old Amazonian forests are more resistant to precipitation variability than shorter, younger, forests but are more susceptible to fluctuations in VPD. Forest height and age thus have an important role in determining the forests' response to interannual precipitation variability.

Interannual variability of the data set

We use canopy height data from spaceborne lidar measurements[27] and Global Precipitation Climatology Project (GPCP) precipitation[28] to evaluate the forest height and precipitation across the Amazon basin. The canopy height metric measures the height of the uppermost level of the forest, ignoring the height of the lower levels[27]. GOME-2 SIF[24] is used as a proxy for photosynthesis. VPD is calculated using relative humidity and temperature from the Atmospheric Infrared Sounder (AIRS)[29]. Tree age and aboveground biomass (AGB) are obtained from data-constrained statistical model estimations[30,31]. Tree-scale isohydricity reflects the degree to which a tree can regulate leaf water potential while environmental conditions (soil water potential and atmospheric evaporative

[1]Department of Earth and Environmental Engineering, Columbia University, New York, NY, USA. [2]École Polytechnique Fédérale de Lausanne, Lausanne, Switzerland. [3]Department of Earth System Science, Stanford University, Stanford, CA, USA. [4]Department of Earth and Environmental Engineering, Columbia University, New York, NY, USA. [5]Departamento de Biologia Vegetal, Universidade Estadual de Campinas, Campinas, Brazil. [6]School of Plant Biology, University of Western Australia, Perth, Western Australia, Australia. [7]Department of Ecology, Evolution and Environmental Biology, Columbia University, New York, NY, USA. [8]The Earth Institute, Columbia University, New York, NY, USA. *e-mail: pg2328@columbia.edu

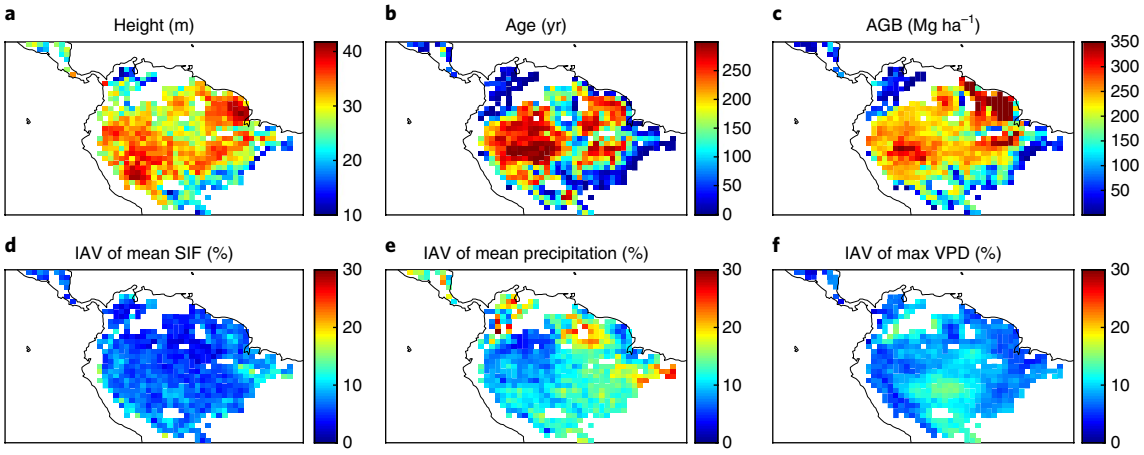

Fig. 1 | Spatial patterns of canopy characteristics and interannual variability of climatic drivers between 2007 and 2015. a, Canopy height. **b**, Tree age. **c**, Aboveground biomass. **d**, Interannual variability of mean SIF. **e**, Interannual variability of mean precipitation. **f**, Interannual variability of maximum VPD. The interannual variabilities are calculated by dividing the interannual standard deviation by the interannual mean. Only data for tropical rainforests are shown. IAV, interannual variability.

demand) are changing[32,33]. Anisohydry is the converse of isohydry, and refers to large variations in leaf water potential. An ecosystem-scale anisohydricity metric was calculated from vegetation optical depth (see Methods). Anisohydricity was estimated as the slope of the temporal regression between midday leaf and soil water potentials[33] (Supplementary Fig. 1c). The leaf water potential of more isohydric ecosystems is less sensitive to declines in soil water potential because of stronger stomatal regulation but also potentially because of a greater reliance on stored water[34].

The spatial distribution of canopy height is not correlated (Fig. 1a) with interannual changes in precipitation, SIF or maximum monthly VPD (Fig. 1d–f, all of which show distinct spatial patterns), but, not surprisingly, height is correlated with age and AGB (Fig. 1b,c). This correlation is confirmed by the coefficients of determination of tree height with age and AGB ($R^2=0.42$, 0.48, Fig. 2a,b).

The negative relationship of anisohydricity with tree height (Fig. 2c, $R^2=0.15$) is consistent with the fact that emergent and canopy tree species tend to close their stomata during peak daytime sunlight hours to avoid leaf desiccation and xylem cavitation, because their xylem vessels are more vulnerable to embolism[23,35]. In other words, taller trees and forests have a more isohydric behaviour[33]. However, we do not expect the correlation to be perfect because of forest biodiversity and because of the noisier nature of the anisohydricity estimates in the Amazon, here an imperfect thermal equilibrium assumption used in the derivation of afternoon VOD adds noise[33]. Tall forests typically also have a deeper rooting depth[1] (see Methods, $R=0.26$, and $R=0.36$ for forests above 30 m), which can better mitigate the drop in soil (and therefore predawn leaf) water potential during dry periods[36] (see Methods, 'Plant hydraulics model').

The correlation of mean annual precipitation with the forest characteristics (age, AGB, anisohydricity, respectively) was small overall ($R^2=0.17$, 0.1 and 0.09, respectively) (Supplementary Fig. 2a-c). Canopy height was nearly independent from, but slightly positively correlated with, mean annual precipitation ($R^2=0.08$, Fig. 2d). Using a hyperbolic curve ($ax/(b+x)$) only marginally increased the fit ($R^2=0.1$). The relationship was negligible in the wetter part of the Amazon ($R^2=0.01$ for mean annual precipitation above 2,000 mm, Fig. 2d) but also over the drier part ($R^2=0.07$ for mean annual precipitation below 2,000 mm, Fig. 2d), further emphasizing that tall forests are not only growing in the wettest regions. In addition, there was no relationship between tree height and soil type (Supplementary Fig. 3). We thus conclude that the effect of forest height on the response to climate variability does not reflect an effect of soil porosity, water holding capacity or mean precipitation.

Analysis of precipitation and VPD sensitivity

In this study, SIF is used as a proxy for GPP, as SIF is directly related to the photosynthesis rate[37], and the relationship with GPP at large spatial and time scales has been shown to be almost linear[38]. SIF can still be captured in the presence of relatively thick cloud cover (see Methods). However, the seasonal correlation between SIF and GPP is naturally weaker in the wet tropics, mostly because of the minimal GPP seasonality and noise in the data[21]. Nevertheless, SIF seasonality in the Amazon is correlated to seasonality of carbon dioxide uptake[39] and canopy near-infrared reflectance from MODIS (Moderate-Resolution Imaging Spectroradiometer)[21]. SIF has also been shown to capture water stress in the Amazon better than commonly used optically based vegetation indices[40].

To study the effect of forest height on the sensitivity of photosynthesis to precipitation and VPD, a nine-year record of SIF, VPD and precipitation was used at a monthly scale for each 1° pixel. A pixel-by-pixel normalization was used for SIF, VPD and precipitation by subtracting and dividing by the interannual mean of each pixel. Monthly SIF and precipitation values were averaged yearly to yield nine values for each pixel. Using annually averaged SIF reduced the impact of month-to-month noise, which typically has little to no autocorrelation. For VPD, the maximum value in each year was used rather than the average, as we are interested in plant sensitivity to extremes of this variable (see Methods). We note, however, that using the mean annual value of VPD yielded similar conclusions, as the VPD annual mean is dominated by the dry season maximum (not shown).

Tall forests are also generally older (Fig. 2a) and have deeper rooting depth (see Methods) with a correlation of forest height with rooting depth of $R=0.26$, and $R=0.36$ for forests above 30 m. The deeper rooting depth of taller forests regulates access to deeper soil moisture, and consequently soil and leaf water potential, on seasonal timescales, which buffers seasonal drying through deep soil moisture[36] (Fig. 2c.). The sensitivity of SIF to precipitation is lower for taller forests, while the sensitivity to VPD is higher (Fig. 3a,b). Photosynthesis in taller forest is three times less sensitive to precipitation interannual variability than in shorter ones. Taller forests are also much more sensitive to VPD than shorter ones (Fig. 3a). These results are confirmed by a soil–plant–atmosphere continuum (SPAC) model (see Methods), which shows that photosynthesis

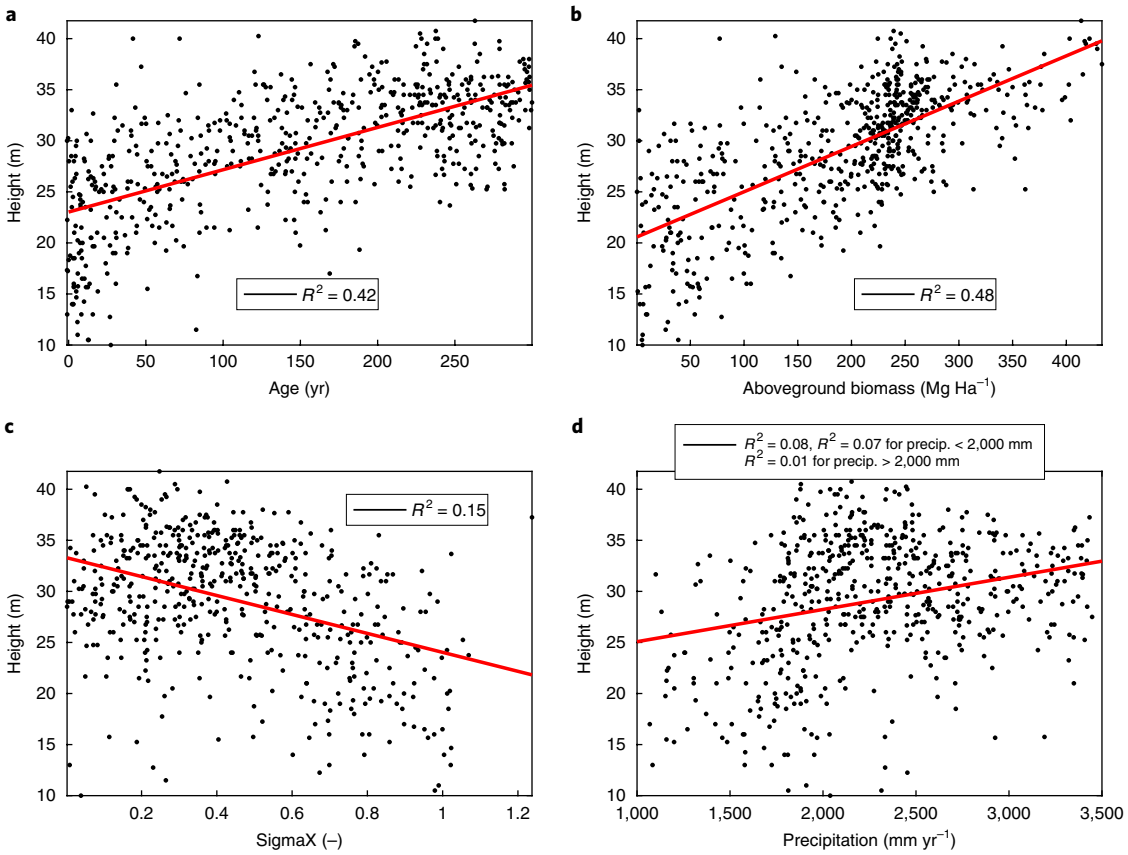

Fig. 2 | Correlation of tree height with canopy characteristics and precipitation. a, Scatter plot for tree height and age. **b**, Scatter plot for tree height and aboveground biomass. **c**, Scatter plot for tree height and degree of anisohydricity (SigmaX). **d**, Scatter plot for tree height and mean interannual precipitation (2007–2015). Coefficients of determination are shown in every plot. The significance of correlation was calculated using a *t*-test with a significance level of 0.05. All correlations are significant at $P < 0.001$.

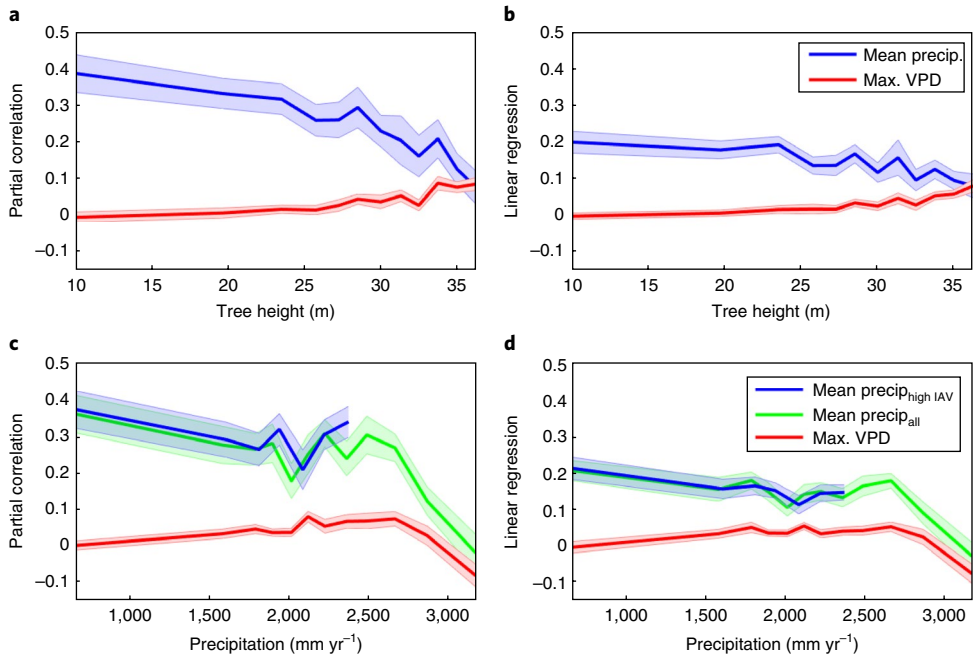

Fig. 3 | Variations of SIF sensitivity to VPD and precipitation binned by tree height and precipitation. a–**d**, Partial correlation (**a**,**c**) and linear regression (**b**,**d**) coefficients for the sensitivity of mean SIF to mean precipitation (blue line) and maximum VPD (red line), binned by tree height (**a**,**b**) and by mean interannual precipitation (**c**,**d**). The green line (mean precip$_{all}$) shows the results, including pixels with a precipitation interannual variability lower than 10%. Normalized yearly values were used for every variable. Confidence intervals were calculated by bootstrapping across each pixel ($n = 2{,}000$). Shading represents confidence intervals, assessed by bootstrapping.

of tall trees is less sensitive to a simulated soil drydown than that of short trees, but more sensitive to increases in VPD (Fig. 3a,b and Supplementary Figs. 4 and 7). The resilience of all trees to modelled drydown was associated primarily with deeper rooting, which utilizes deep soil moisture to buffer seasonal drying (Supplementary Fig. 4). A second mechanism was also observed, associated with the relative effects of decreasing the soil potential on the soil-to-root hydraulic gradient for tall and short trees. Tall trees routinely experience lower leaf water potentials because of their long xylem hydraulic path (and a larger gradient in water potential from soil to root), so photosynthesis is less sensitive to drying (Supplementary Fig. 4), because the loss in potential gradient due to a given decrease soil water potential is relatively smaller than for shorter trees (Supplementary Fig. 6). Conversely, due to lower soil-to-root conductance, tall trees are more sensitive to VPD fluctuations (Supplementary Fig. 7). There was a very small relationship between tree height and VPD ($R^2 = 0.09$), so we can conclude that taller trees were not necessarily growing in low VPD regions.

Besides forest height, we also tested whether mean precipitation has a control on photosynthesis, based on its effect on photosynthesis seasonality. Unlike forest height, there is no trend (and thus no nonlinearity) in SIF sensitivity with changing mean precipitation bin, emphasizing that productivity, as assessed by SIF, responded nearly linearly to mean precipitation (Fig. 3c,d). The SIF response is almost flat, oscillating around a correlation value of 0.3. Performing a linear regression instead of a partial correlation did not change the final outcome (Fig. 3b,d), although the coefficients are slightly smaller in magnitude. We note that the right tail (that is, points $>2{,}500\,mm\,yr^{-1}$) of the precipitation-binned graphs is spurious (Fig. 3c,d, green lines). The points in these bins show an interannual precipitation variability lower than 10% (Fig. 1e, dark blue area in the northeastern Amazon) and thus primarily add noise to the analysis. That is, no relationship with SIF can be deduced from the pixels with no precipitation variability, as there is not sufficient precipitation forcing to assess the SIF response.

The analysis was repeated excluding 2015 to test the influence of this intense El Niño year on our findings; this yielded similar results (Supplementary Fig. 1a), emphasizing that the response of precipitation variability as a function of forest height did not change during extreme droughts. Other water stress indices such as cumulative water deficit (CWD) or the standardized precipitation–evapotranspiration index (SPEI) were very highly correlated with annual precipitation (see Methods and Supplementary Fig. 8), so total annual precipitation was considered a good indicator of water supply for the year.

We also binned by degree of anisohydricity to gain insight directly into the impact of tree hydraulics. SIF was less sensitive to interannual precipitation for taller forests, which, despite being more isohydric, also have deeper rooting depths (see Methods) that mitigate declines in soil water potential. However, the noise in the anisohydricity data set over the Amazon and biodiversity affected the quality of the relationship between SIF and anisohydricity (Supplementary Fig. 1b).

Increased surface radiation during dry periods could impact available photosynthetically active radiation and potential evaporation[41], which can in turn modify evaporation and photosynthesis. The inclusion of incoming shortwave radiation at the surface had a relatively small effect on the estimated precipitation and VPD sensitivities, mostly adding noise (Supplementary Fig. 9). Remotely sensed radiation, especially at the surface, is difficult to retrieve in this area because of clouds. In fact, the CERES product is calculated by measuring top-of-atmosphere radiation, using atmospheric models to simulate the effects of clouds on surface shortwave radiation, which are highly uncertain[42]. The lack of effect of including shortwave radiation is nonetheless consistent with the low interannual variability of the shortwave radiation (Supplementary Fig. 10d), the low correlation between shortwave radiation and SIF (Supplementary Fig. 11c,f,i) and the SIF sensitivity to shortwave radiation (Supplementary Fig. 12).

Relationship to in situ experiments

The higher resistance to precipitation of tall and old forests compared to shorter and younger ones is consistent with recent observations comparing the response of individual trees during a precipitation exclusion experiment in the Amazon[23]. Interannual variability in the growth of taller trees was found to be lower under drought as compared to smaller trees; that is, the growth of taller trees is maintained during drought. Taller forests are more vulnerable to atmospheric aridity and need to regulate their stomata to avoid desiccation during sunlight peak hours (Supplementary Fig. 7)[33]. Despite their increased isohydry, taller forests are less sensitive to scarce precipitation compared to smaller trees. This could be due to deeper rooting (which mitigates the effect on soil potential) and/or generally larger gradients in water potential from soil to root (whereby losses due to isohydry are a relatively small portion of the total gradient; see Methods, 'Plant hydraulics model'). Future research is needed to disentangle the effects of plant rooting depth, hydraulic conductance, stomatal closure, stored water and tree vulnerability on this response to VPD and precipitation deficit.

Our results demonstrate that in the Amazon, forest height and age regulate photosynthesis interannual variability and are as relevant as mean precipitation. In particular, tall, old and dense forests are more resistant to precipitation variability. Tree size and age directly impact forest structure and thus the carbon cycle in the Amazon[43]. This is especially significant given the importance of the Amazon rainforest, not only for the global carbon cycle[2], but also for global atmospheric circulation, which is closely connected to the evapotranspiration process of this area[44]. Forest height, age and biomass have a role equivalent to mean precipitation in the regulation of forest photosynthesis response to interannual climate variability.

Methods

Methods, including statements of data availability and any associated accession codes and references, are available at https://doi.org/10.1038/s41561-018-0133-5.

Received: 24 August 2017; Accepted: 16 April 2018;
Published online: 28 May 2018

References

1. Sternberg, L. et al. Root distribution in an Amazonian seasonal forest as derived from $\delta^{13}C$ profiles. *Plant Soil* **205**, 45–50 (1998).
2. Pan, Y. et al. A large and persistent carbon sink in the world's forests. *Science* **333**, 988–993 (2011).
3. Betts, R. et al. The role of ecosystem–atmosphere interactions in simulated Amazonian precipitation decrease and forest dieback under global climate warming. *Theor. Appl. Climatol.* **78**, 157–175 (2004).
4. Friedlingstein, P. et al. Climate–carbon cycle feedback analysis: results from the C^4MIP model Intercomparison. *J. Clim.* **19**, 3337–3353 (2006).
5. Jiménez-Muñoz, J. C. et al. Record-breaking warming and extreme drought in the Amazon rainforest during the course of El Niño 2015–2016. *Sci. Rep.* **6**, 5204 (2016).
6. Espinoza, J. C. et al. Climate variability and extreme drought in the upper Solimões River (western Amazon Basin): understanding the exceptional 2010 drought. *Geophys. Res. Lett.* **38**, L13406 (2011).
7. Brando, P. M. et al. Seasonal and interannual variability of climate and vegetation indices across the Amazon. *Proc. Natl Acad. Sci. USA* **107**, 14685–14690 (2010).
8. Phillips, O. L. et al. Drought sensitivity of the Amazon rainforest. *Science* **323**, 1344–1347 (2009).
9. Doughty, C. E. et al. Drought impact on forest carbon dynamics and fluxes in Amazonia. *Nature* **519**, 78–82 (2015).
10. Feldpausch, T. R. et al. Amazon forest response to repeated droughts. *Glob. Biogeochem. Cycles* **30**, 964–982 (2016).
11. Gatti, L. V. et al. Drought sensitivity of Amazonian carbon balance revealed by atmospheric measurements. *Nature* **506**, 76–80 (2014).

12. Lewis, S. L., Brando, P. M., Phillips, O. L., van der Heijden, G. M. F. & Nepstad, D. The 2010 Amazon drought. *Science* **331**, 554–554 (2011).
13. Saleska, S. R., Didan, K., Huete, A. R. & da Rocha, H. R. Amazon forests green-up during 2005 drought. *Science* **318**, 612 (2007).
14. Samanta, A. et al. Amazon forests did not green-up during the 2005 drought. *Geophys. Res. Lett.* **37**, L13406 (2010).
15. Morton, D. C. et al. Amazon forests maintain consistent canopy structure and greenness during the dry season. *Nature* **506**, 221–224 (2014).
16. Wu, J. et al. Leaf development and demography explain photosynthetic seasonality in Amazon evergreen forests. *Science* **351**, 972–976 (2016).
17. Guan, K. et al. Photosynthetic seasonality of global tropical forests constrained by hydroclimate. *Nat. Geosci.* **8**, 284–289 (2015).
18. Konings, A. G., Williams, A. P. & Gentine, P. Sensitivity of grassland productivity to aridity controlled by stomatal and xylem regulation. *Nat. Geosci.* **7**, 2193–2197 (2017).
19. Novick, K. A. et al. The increasing importance of atmospheric demand for ecosystem water and carbon fluxes. *Nat. Clim. Change* **6**, 1023–1027 (2016).
20. Williams, A. P. Temperature as a potent driver of regional forest drought stress and tree mortality. *Nat. Clim. Change* **3**, 292–297 (2012).
21. Xu, L. et al. Satellite observation of tropical forest seasonality: spatial patterns of carbon exchange in Amazonia. *Environ. Res. Lett.* **10**, 084005 (2015).
22. Maeda, E. E., Kim, H., Aragão, L. E. O. C., Famiglietti, J. S. & Oki, T. Disruption of hydroecological equilibrium in southwest Amazon mediated by drought. *Geophys. Res. Lett.* **42**, 7546–7553 (2015).
23. Rowland, L. et al. Death from drought in tropical forests is triggered by hydraulics not carbon starvation. *Nature* **528**, 119–122 (2015).
24. Joiner, J. et al. Global monitoring of terrestrial chlorophyll fluorescence from moderate-spectral-resolution near-infrared satellite measurements: methodology, simulations, and application to GOME-2. *Atmos. Meas. Tech.* **6**, 2803–2823 (2013).
25. Frankenberg, C. et al. New global observations of the terrestrial carbon cycle from GOSAT: patterns of plant fluorescence with gross primary productivity. *Geophys. Res. Lett.* **38**, L7706 (2011).
26. Green, J. K. et al. Regionally strong feedbacks between the atmosphere and terrestrial biosphere. *Nat. Geosci.* **48**, 410–422 (2017).
27. Simard, M., Pinto, N., Fisher, J. B. & Baccini, A. Mapping forest canopy height globally with spaceborne lidar. *J. Geophys. Res.* **116**, G04021 (2011).
28. Huffman, G. J. et al. Global precipitation at one-degree daily resolution from multisatellite observations. *J. Hydrometeorol.* **2**, 36–50 (2001).
29. Aumann, H. H. & Pagano, R. J. Atmospheric infrared sounder on the Earth observing system. *Opt. Eng.* **33**, 776–784 (1994).
30. Chazdon, R. L. et al. Carbon sequestration potential of second-growth forest regeneration in the Latin American tropics. *Proc. Natl Acad. Sci. USA* **2**, e1501639 (2016).
31. Avitabile, V. et al. An integrated pan-tropical biomass map using multiple reference datasets. *Glob. Change Biol.* **22**, 1406–1420 (2016).
32. Martinez-Vilalta, J., Poyatos, R., Aguadé, D., Retana, J. & Mencuccini, M. A. A new look at water transport regulation in plants. *New Phytol.* **204**, 105–115 (2014).
33. Konings, A. G. & Gentine, P. Global variations in ecosystem-scale isohydricity. *Glob. Change Biol.* **23**, 891–905 (2017).
34. Domec, J.-C. & Johnson, D. M. Does homeostasis or disturbance of homeostasis in minimum leaf water potential explain the isohydric versus anisohydric behavior of *Vitis vinifera* L. cultivars? *Tree Physiol.* **32**, 245–248 (2012).
35. Brodribb, T. J., Holbrook, N. M., Edwards, E. J. & Gutierrez, M. V. Relations between stomatal closure, leaf turgor and xylem vulnerability in eight tropical dry forest trees. *Plant Cell Environ.* **26**, 443–450 (2003).
36. Martinez-Vilalta, J. & Garcia-Forner, N. Water potential regulation, stomatal behaviour and hydraulic transport under drought: deconstructing the iso/anisohydric concept. *Plant Cell Environ.* **40**, 962–976 (2016).
37. Porcar-Castell, A. et al. Linking chlorophyll a fluorescence to photosynthesis for remote sensing applications: mechanisms and challenges. *J. Exp. Bot.* **65**, 4065–4095 (2014).
38. Zhang, Y. et al. Consistency between sun-induced chlorophyll fluorescence and gross primary production of vegetation in North America. *Remote Sens. Environ.* **183**, 154–169 (2016).
39. Parazoo, N. C. et al. Interpreting seasonal changes in the carbon balance of southern Amazonia using measurements of XCO_2 and chlorophyll fluorescence from GOSAT. *Geophys. Res. Lett.* **40**, 2829–2833 (2013).
40. Lee, J. E. et al. Forest productivity and water stress in Amazonia: observations from GOSAT chlorophyll fluorescence. *Proc. R. Soc. B* **280**, 20130171 (2013).
41. Anber, U., Gentine, P., Wang, S. & Sobel, A. H. Fog and rain in the Amazon. *Proc. Natl Acad. Sci. USA* **112**, 11473–11477 (2015).
42. Wielicki, B. et al. Clouds and the Earth's Radiant Energy System (CERES): an Earth observing system experiment. *BAMS* **77**, 853–868 (2000).
43. Meakem, V. et al. Role of tree size in moist tropical forest carbon cycling and water deficit responses. *New Phytol.* https://doi.org/10.1111/nph.14633 (2017).
44. Malhi, Y. et al. Exploring the likelihood and mechanism of a climate-change-induced dieback of the Amazon rainforest. *Proc. Natl Acad. Sci. USA* **106**, 20610–20615 (2009).

Acknowledgements

The authors thank Columbia Water Center for comments, in particular J. Green. The authors also thank the providers of the other data sets used in this study.

Author contributions

F.G., D.K., A.G.K. and P.G. wrote the main manuscript text. F.G., P.G., D.K. and S.H.A. prepared figures. F.G., P.G. and A.G.K. designed the study. F.G., D.K., A.G.K., M.U. and R.S.O. reviewed and edited the manuscript. D.K. performed the plant hydraulics simulations.

Competing interests

The authors declare no competing interests.

Additional information

Supplementary information is available for this paper at https://doi.org/10.1038/s41561-018-0133-5.

Reprints and permissions information is available at www.nature.com/reprints.

Correspondence and requests for materials should be addressed to P.G.

Publisher's note: Springer Nature remains neutral with regard to jurisdictional claims in published maps and institutional affiliations.

Methods

Data sets. SIF, precipitation, surface incoming shortwave radiation and VPD data are all taken from empirical remotely sensed data sets. SIF is from version 2.6 of GOME-2[24], precipitation is from version 1.2 of GPCP[28], surface incoming shortwave radiation is from CERES[42], and VPD was calculated using temperature and relative humidity from version 6 of AIRS[29]. All remote-sensing data sets were used at monthly resolution. In the analysis, we used mean annual precipitation as an indicator of water stress. More complex dryness indicators such as CWD or SPEI are extremely correlated with annual precipitation (Supplementary Fig. 8), as interannual variations in radiation and evaporative demand are small (Supplementary Fig. 10). We thus chose mean annual precipitation as our main dryness indicator as it is simpler to quantitatively understand.

The land cover data are from the MCD12C1 product[45]. The canopy height metric was derived from spaceborne lidar measurements and validated by field measurements, with an increased accuracy in the Amazon compared to previous metrics[27]. The degree of anisohydricity metric at the ecosystem scale was calculated based on the long-term diurnal variations in microwave vegetation optical depth, which are dependent on vegetation water content[33]. A temporally fixed value of anisohydricity was used for every pixel and is thus not impacted by the specific interannual variability in precipitation, especially during El Niño years[33]. AGB was obtained by combining high-resolution biomass maps with a reference data set of field observations[31,46], whereas mean forest age was estimated using a 500-m-resolution map of forest biomass and an equation connecting biomass to forest age[30,47].

The satellite record availability was from January 2007 to January 2016, even though a longer data record would yield more accurate results. Although some data sets were available at a finer resolution, a common grid resolution of 1°×1° was used for consistency. The original resolution and spatial extent of the age and AGB data set did not match the other data sets, so some approximations were necessary to convert them. For example, after upscaling to the 1°×1° grid resolution, the latitude limits of the age and AGB data sets were rounded from [−23.4039, 23.400] to [−23.5, 23.5], possibly leading to some errors.

Monthly SIF can be noisy, especially in the presence of clouds and because the influence of the South Atlantic Anomaly limits the number of available measurements of the surface[24]. The monthly averages of SIF are only computed on days when the effective cloud fraction is <30%. Note that the effective cloud fraction, which is estimated using a model that uses cloud reflectance and albedo as inputs[48–50], is generally lower than the geometric one. In a given pixel, it is still possible to detect up to 80% of the SIF signal with a cloud optical thickness equal to up to 10 and a true cloud fraction of 40%[51]. Additionally, varying the effective cloud fraction threshold between 0 and 50% produced only slight differences in the spatial and temporal patterns of SIF[24]. We thus assume this cloud filtering to cause a minimal error at the monthly scale. Using the annual mean SIF anomalies in lieu of only monthly values reduces the inherent noise in SIF, as monthly observational remote sensing errors can be assumed to be independent. SIF can capture interannual variability in photosynthesis over the Amazon basin and in particular it has been shown to correctly observe water stress in the Amazon, unlike typical vegetation indices[40].

The data sets were complemented by a recent global estimate of rooting depth, based on the inversion of an ecohydrological model combined with water table estimates, and extensively validated using rooting depth observations from the literature[52] (Supplementary Fig. 14). Although this data set is the best estimate of variability in rooting depth across the Amazon currently available, it is important to recognize that its quality highly depends on the accuracy of the ecohydrological model used in the inversion, and that this data set is probably somewhat noisy in a poorly understood region like the Amazon.

Study site. The original data set was cropped to 15.5° N–19.5° S latitude to focus on the tropics. After excluding Congo and Indonesia from the analysis, the longitude was also limited to 95.5° W–40.5° W. Rainforest areas were delineated using a combination of high canopy heights (greater than 25 m)[52] and high average SIF (greater than 1 mW m^{-2} nm^{-1} sr^{-1}). After filtering, some isolated pixels in the southwest of the Amazon rainforest were still erroneously included; they were then removed from the analysis. Land cover data were used to mask the ocean pixels close to coastlines. All pixels consisting of more than 75% land area were then considered as land-covered.

Originally, the analysis was also performed in the Congolese and Indonesian rainforests. However, the low SIF interannual variability in Congo (Supplementary Fig. 10a) caused the SIF signal-to-noise ratio to be too low to use this region in our study. In Indonesia, the observed SIF interannual variability is higher (Supplementary Fig. 10a). However, the geography of the area made the distinction between ocean and land pixels complicated. After filtering out the ocean pixels, there were too few pixels left to perform the analysis. Both forests were discarded in the end, and we focused solely on the Amazon.

Statistical analysis. Negative SIF values were assumed to originate from measurement errors and excluded from the analysis. Canopy height values equal to zero were also excluded, in addition to pixels with an average interannual precipitation greater than 4,000 mm yr^{-1}, as these were considered outliers. To explore the data before performing the analysis, the interannual variability of the climatic drivers was calculated by dividing the interannual standard deviation by the interannual mean (Fig. 1d–f and Supplementary Fig. 10).

The data were then binned by canopy height and precipitation (Fig. 3). Due to the small number of observations, a constant bin size of 50 pixels was selected, a compromise between having enough pixels per bin and enough points in the final graph (that is, number of bins) (Fig. 3). For each pixel, the monthly values of SIF, VPD and precipitation were normalized by subtracting and dividing by their interannual averages. Normalizing allows us to offset the variations in average SIF, VPD and precipitation across pixels beyond meteorological forcing. The SIF and precipitation annual means were calculated, as well as the VPD annual maximum. A partial correlation (Fig. 3a,c) and linear regression (Fig. 3b,d) were computed independently for each bin between precipitation, VPD and SIF. It is difficult to disentangle the effects of VPD from precipitation; the VPD annual maximum was preferred over the annual mean as it is less correlated with the mean annual precipitation (Supplementary Fig. 1d and Supplementary Fig. 13e,h), so their effects on SIF can be considered separately. Precipitation pixels with an interannual variability value lower than 10% only added noise to the analysis. For this reason, results excluding those pixels are shown in the foreground (Fig. 3c,d, '$precip_{highIAV}$' blue line). When binning by canopy height, this problem does not occur as the pixels inside each bin have mixed interannual variabilities (Fig. 1 and Supplementary Figs. 11 and 13).

Because of spatial and temporal autocorrelation in each of the variables, uncertainty intervals were determined using bootstrapping, rather than statistical tests, which tend to assume identical and independent distributions. For each regression, confidence intervals were built by bootstrapping with 2,000 realizations across each pixel. The standard deviation of the correlation or linear regression coefficients of the 2,000 realizations was used as the confidence interval.

Plant hydraulics model. Our remote sensing results were combined with a simplified SPAC model to gain physical intuition into the results. In this model, soil water potential is imposed and transpiration demand is based on Penman–Monteith and the Medlyn stomatal conductance model. The forcing data are based on the diurnal course of a day during the dry season in the wet part of the Amazon. The forcing weather station data is from the K34 flux tower, in Brazil for the month of September. The model uses a photosynthesis model based on recent optimization theory[53], which has been shown to work well across plant types.

Sap flow q in the model is based on the integral of the hydraulic conductivity across the plant potentials, from the soil ψ_s to the leaf ψ_l:

$$q = \int_{\psi_s}^{\psi_l} \frac{K(\psi)}{z} \mathrm{d}\psi \tag{1}$$

Xylem conductance is the ratio of specific conductivity K, a function of local xylem potential ψ because of loss of conductivity in the xylem through cavitation, to tree height z. We assume a simplified linearized loss of conductivity in the xylem from its maximum value K_{max} to zero:

$$K(\psi) = K_{\max} min\left(max\left(\frac{\psi - p_2}{p_1 - p_2}, 0\right), 1\right) \tag{2}$$

Non hydraulics-limited stomatal conductance is based on Medlyn's empirical-optimal model[53]:

$$g_{c,\max} = g_0 + \left(1 + \frac{g_1}{\sqrt{\mathrm{VPD}}}\right)\frac{A}{c_a} \tag{3}$$

where A is net assimilation, c_a is atmospheric ambient CO_2 concentration, VPD is vapour-pressure deficit, g_0 is the minimum stomatal conductance and g_1 is an underlying water use efficiency parameter. Stomatal conductance is modulated by leaf water potential drop as

$$g_c = g_{c,\max} h(\psi_l) \tag{4}$$

whereby stomatal conductance decreases relative to maximal values with increasingly negative leaf water potential (following ref. [54]), subject to two parameters, p_{50} (leaf water potential at 50% loss of stomatal conductance) and a (sigmoidal shape-fitting parameter):

$$h(\psi_l) = \frac{1}{1 + \left(\frac{\psi_{leaf}}{p_{50}}\right)^a} \tag{5}$$

Soil potential is modelled using a simplified single-layer bucket model, where soil water balance is carried out over a single layer over the effective rooting depth (Z_r) with evapotranspiration (q) as the only outflow:

$$\theta_1 = \theta_0 - \frac{q\Delta t}{Z_r} \tag{6}$$

Soil water retention is modelled following a typical empirical formula[55,56]:

$$\psi_{soil}(\theta) = \psi_{soil,sat}\left(\frac{\theta}{\theta_{sat}}\right)^{-b} \quad (7)$$

The model is solved in three consecutive steps. First, the model solves the maximum canopy conductance and assimilation, iterating on intercellular CO_2. The model then solves the leaf water potential, which reflects a balance between sap flow and transpiration, given by Penman–Monteith transpiration with the adjusted stomatal conductance based on $h(\psi_l)$. Finally, soil potential is updated and the photosynthesis module is called again to calculate assimilation reflecting hydraulic limitations, iterating on intercellular CO_2. The model is iterated until convergence at every step. Parameters for the SPAC model are based on tropical rainforest data. The only differences between the short and tall forest simulations are the height (z), rooting depth (Z_r) and the point of 50% loss of stomatal conductivity (p_{50}), which is modified to reflect a constant safety margin across ecosystems, as plants tend to make full use of their xylem conductivity by operating at a low safety margin[57]. Other parameters are kept constant. Three 60 day drydowns are used to evaluate the sensitivity to soil and atmospheric drying (Supplementary Figs. 4–7).

Data availability. All data used in this study are openly available from the following: GOME-2 SIF; https://avdc.gsfc.nasa.gov/pub/data/satellite/MetOp/GOME_F; canopy height: https://webmap.ornl.gov/ogc/wcsdown.jsp?dg_id=10023_1; GPCP precipitation; https://precip.gsfc.nasa.gov/gpcp_daily_comb.html; CERES surface shortwave flux down (All Sky): https://ceres-tool.larc.nasa.gov/ord-tool/jsp/EBAFSFCSelection.jsp; AIRS VPD: https://disc.sci.gsfc.nasa.gov/AIRS/data-holdings/by-data-product-V6; isohydricity data: http://github.com/agkonings/isohydricity; AGB data: http://www.wur.nl/en/Expertise-Services/Chair-groups/Environmental-Sciences/Laboratory-of-Geo-information-Science-and-Remote-Sensing/Research/Integrated-land-monitoring/Forest_Biomass/Forest-Biomass-downloads.htm; MCD12C1 land cover: https://lpdaac.usgs.gov/dataset_discovery/modis/modis_products_table/mcd12c1. The rooting depth data set is available at https://wci.earth2observe.eu/. The soil database is available at https://www.embrapa.br/en/solos. The canopy age data set is available from the corresponding author upon reasonable request. Processed data used in the intermediate steps of the study are available upon request.

References

45. Friedl, M. A. et al. MODIS Collection 5 global land cover: algorithm refinements and characterization of new datasets. *Remote Sens. Environ.* **114**, 168–182 (2010).
46. Santoro, M. et al. Forest growing stock volume of the northern hemisphere: spatially explicit estimates for 2010 derived from Envisat ASAR. *Remote Sens. Environ.* **168**, 316–334 (2015).
47. Baccini, A. et al. Estimated carbon dioxide emissions from tropical deforestation improved by carbon-density maps. *Nat. Clim. Change* **2**, 182–185 (2012).
48. Koelemeijer, R. B. A., Stammes, P., Hovenier, J. W. & de Haan, J. F. A fast method for retrieval of cloud parameters using oxygen A band measurements from the Global Ozone Monitoring Experiment. *J. Geophys. Res.* **106**, 3475–3490 (2001).
49. Stammes, P. et al. Effective cloud fractions from the Ozone Monitoring Instrument: theoretical framework and validation. *J. Geophys. Res.* **113**, D05204–D05212 (2008).
50. Joiner, J. et al. The seasonal cycle of satellite chlorophyll fluorescence observations and its relationship to vegetation phenology and ecosystem atmosphere carbon exchange. *Remote Sens. Env.* **152**, 375–391 (2014).
51. Joiner, J. et al. Filling-in of near-infrared solar lines by terrestrial fluorescence and other geophysical effects: simulations and space-based observations from SCIAMACHY and GOSAT. *Atmos. Meas. Tech.* **5**, 809–829 (2012).
52. Feldpausch, T. R. et al. Height–diameter allometry of tropical forest trees. *Biogeosciences* **8**, 1081–1106 (2011).
53. Medlyn, B. E. et al. Reconciling the optimal and empirical approaches to modelling stomatal conductance. *Glob. Change Biol.* **17**, 2134–2144 (2011).
54. Xu, X., Medvigy, D., Powers, J. S., Becknell, J. M. & Guan, K. Diversity in plant hydraulic traits explains seasonal and inter-annual variations of vegetation dynamics in seasonally dry tropical forests. *New Phytol.* **212**, 80–95 (2016).
55. Corey, A. & Brooks, R. Drainage characteristics of soils. *Soil Sci. Soc. Am. J.* **39**, 251–255 (1975).
56. Brooks, R. & Corey, A. *Hydraulic properties of porous media* Hydrology Paper 3 (Colorado State University, 1964).
57. Gleason, S. M. et al. Weak tradeoff between xylem safety and xylem-specific hydraulic efficiency across the world's woody plant species. *New Phytol.* **209**, 123–136 (2015).